Biomedicine & Pharmacotherapy 193 (2025) 118798

Contents lists available at ScienceDirect

Biomedicine & Pharmacotherapy

journal homepage: www.elsevier.com/locate/biopha

KN21, a direct AMPK activator, alleviates hepatic steatosis and fibrosis by modulating long-chain TAG and pyrimidine metabolism in a MASH mouse model

Jueun Lee [a,1], Seojeong Kim [b,1], Yeajin Ju [a,b,1], Minjung Seo [b], Hyeri Kim [a,b], Jae-Ho Shin [c], Younghwa Na [c], Youngjoo Kwon [b,d,*], Geum-Sook Hwang [a,e,**]

[a] Integrated Metabolomics Research Group, Metropolitan Seoul Center, Korea Basic Science Institute, Seoul 03759, Republic of Korea
[b] College of Pharmacy, Graduate School of Pharmaceutical Sciences, Ewha Womans University, Seoul 03760, Republic of Korea
[c] College of Pharmacy, CHA University, Pocheon 487-010, Republic of Korea
[d] Gradutate Program in Innovative Biomaterials Convergence, Ewha Womans University, Seoul 03760, Republic of Korea
[e] College of Pharmacy, Chung-Ang University, Seoul 06911, Republic of Korea

ARTICLE INFO

Keywords:
MASH
Steatosis
Fibrosis
AMPK activator
Metabolomics
Lipidomics

ABSTRACT

Metabolic dysfunction-associated steatohepatitis (MASH) is a severe form of metabolic dysfunction-associated steatotic liver disease (MASLD) that is characterized by hepatic steatosis, inflammation, and fibrosis and can progress to cirrhosis and hepatocellular carcinoma. AMP-activated protein kinase (AMPK) is a critical regulator of cellular energy homeostasis and has emerged as a promising therapeutic target for MASH. This study aimed to evaluate the mechanism of action of KN21, a novel direct AMPK activator, in a diet-induced MASH mouse model to support its therapeutic potential. C57BL6J mice were fed a choline-deficient, L-amino acid-defined high-fat diet (CDAHFD) to induce MASH, followed by treatment with KN21. Metabolomic and lipidomic profiling were performed using liquid chromatography-mass spectrometry. Histological, biochemical, and molecular analyses were conducted to assess hepatic steatosis and fibrosis. KN21 treatment significantly promoted hepatic AMPK phosphorylation, reduced the liver-to-body weight ratio, mitigated hepatic steatosis, and decreased fibrosis in CDAHFD-fed mice. Lipidomic analysis revealed that KN21 reduced long-chain triacylglycerol (TAG) accumulation, whereas metabolomic analysis revealed that the abundance of pyrimidine metabolites, especially uridine and uracil, was restored in CDAHFD-fed mice. These changes were strongly correlated with reduced fibrotic marker levels, suggesting that KN21 attenuates both lipid accumulation and fibrosis, which are associated with TAG and pyrimidine metabolism and homeostasis. KN21 effectively reduced hepatic steatosis and fibrosis in a diet-induced MASH mouse model through AMPK activation, accompanied by modulation and restoration of long-chain TAG and pyrimidine metabolism. These findings highlight its potential as a promising therapeutic strategy for MASH and provide new insights into the metabolic mechanisms underlying AMPK-mediated hepatoprotection.

Abbreviations: ACC, acetyl-CoA carboxylase; AMPK, AMP-activated protein kinase; CDAHFD, choline-deficient, L-amino acid-defined high-fat diet; COL1A1, collagen type I alpha 1 chain; COL3A1, collagen type III alpha 1 chain; ACTA2, actin alpha 2; PDGFA, platelet-derived growth factor subunit A; PDGFB, platelet-derived growth factor subunit B; ECM, extracellular matrix; SREBF, sterol regulatory element-binding protein; CD36, cluster of differentiation 36; SLC27A2, solute carrier family 27 member 2; PPARα, peroxisome proliferator-activated receptor alpha; PPARβ, peroxisome proliferator-activated receptor beta; PPARγ, peroxisome proliferator-activated receptor gamma; FAS, fatty acid synthase; DNL, *de novo* lipogenesis; FAO, fatty acid oxidation; LCFA, long-chain fatty acid; MASLD, metabolic dysfunction-associated steatotic liver disease; MASH, metabolic dysfunction-associated steatohepatitis; UPLC-QTOF MS, ultra-performance liquid chromatography quadrupole-time-of-flight mass spectrometry; VLCFA, very long-chain fatty acid; FFA, free fatty acid; LysoPC, lysophosphatidylcholine; PC, phosphatidylcholine; LysoPE, lysophosphatidylethanolamine; PE, phosphatidylethanolamine; PG, phosphatidylglycerol; PI, phosphatidylinositol; PS, phosphatidylserine; SM, sphingomyelin; Cer, ceramide; DAG, diacylglycerol; TAG, triacylglycerol; TAGs-SCFA, triacylglycerols with short-chain fatty acid; TAGs-LCFA, triacylglycerols with long-chain fatty acid.

* Corresponding author at: College of Pharmacy, Graduate School of Pharmaceutical Sciences, Ewha Womans University, Seoul 03760, Republic of Korea.
** Corresponding author at: Integrated Metabolomics Research Group, Metropolitan Seoul Center, Korea Basic Science Institute, Seoul 03759, Republic of Korea.
E-mail addresses: ykwon@ewha.ac.kr (Y. Kwon), gshwang@kbsi.re.kr (G.-S. Hwang).
[1] These authors contributed equally to this work and share first authorship

https://doi.org/10.1016/j.biopha.2025.118798
Received 8 September 2025; Received in revised form 8 November 2025; Accepted 18 November 2025
Available online 21 November 2025
0753-3322/© 2025 The Author(s). Published by Elsevier Masson SAS. This is an open access article under the CC BY-NC-ND license (http://creativecommons.org/licenses/by-nc-nd/4.0/).

1. Introduction

Metabolic dysfunction-associated steatotic liver disease (MASLD) is a prevalent liver disorder characterized by excessive hepatic lipid accumulation and is increasing in incidence worldwide, affecting approximately 25 % of the global population [1]. The progressive form of MASLD, known as metabolic dysfunction-associated steatohepatitis (MASH), is distinguished by hepatic inflammation, hepatocellular ballooning, and progressive fibrosis. Over time, MASH can lead to cirrhosis, hepatocellular carcinoma, and liver-related mortality [2]. Despite extensive research on pharmacological interventions targeting *de novo* lipogenesis (DNL) and enzymes that regulate fibrosis in the context of MASLD and MASH, effective treatment options remain limited [3–6]. To date, resmetirom, a thyroid hormone receptor beta agonist, is the only FDA-approved drug for noncirrhotic nonalcoholic steatohepatitis, having received approval in 2024 [7].

AMP-activated protein kinase (AMPK) is a master regulator of cellular energy homeostasis and plays a central role in metabolic disorders such as insulin resistance and dyslipidemia [8]. Notably, AMPK activity is often downregulated in MASH, contributing to impaired lipid metabolism and accelerated disease progression [9]. Given its pivotal role in maintaining hepatic metabolic balance, AMPK activation has emerged as a promising therapeutic strategy for MASLD and MASH [10]. AMPK activation in the liver not only inhibits DNL but also promotes fatty acid oxidation and enhances mitochondrial function, thereby reducing the risk of MASLD progression [11].

Metabolomics, a key area of study in the "omics" sciences—including genomics, transcriptomics, and proteomics—offers valuable insights into the metabolic pathways involved in physiological and pathological processes by profiling metabolites in cells, tissues, and biofluids. As a specialized subfield within metabolomics, lipidomics provides a comprehensive analysis of lipid species, including glycerolipids, phospholipids, sphingolipids, fatty acids, and steroids, which are involved in various biological processes such as metabolism, energy storage, inflammation, cell signaling, and cell membrane integrity. Since hepatic metabolic reprogramming occurs during the onset and progression of MASLD to MASH, metabolomics and lipidomics are powerful tools for investigating the underlying disease mechanisms and identifying novel therapeutic targets.

Previous studies have successfully applied these approaches to identify metabolic and lipidomic alterations associated with potential therapeutics for metabolic disorders, obesity, and MASH. For example, lipidomic profiling has demonstrated that pioglitazone, a thiazolidinedione drug that acts as a PPARγ ligand, alleviates hepatic steatosis in an obesity and type 2 diabetes rat model by modulating lipid metabolism. This effect is mediated through alterations in free fatty acids, lysophosphatidylcholine, phosphatidylcholine, and phospholipase A2, thereby inhibiting DNL and hepatic lipid accumulation [12]. Similarly, lipidomic analysis has revealed the mechanism of action through which Yijin-Tang, a traditional herbal remedy, alleviates systemic inflammation and insulin resistance using plasma lipidomic profiles from obese mice [13]. Additionally, valproic acid has been identified as an AMPK activator, and its metabolic effects have been confirmed through metabolomics analysis of the liver tissues of obese mice [14]. Despite these advances, the specific metabolic and lipidomic alterations associated with AMPK-targeted therapies in MASH remain largely unexplored.

In this study, we utilized the choline-deficient, L-amino acid-defined high-fat diet (CDAHFD) model, a well-established and widely used model in MASH research that effectively recapitulates the robust fibrosis observed in human MASH [15,16]. However, the CDAHFD model can induce weight loss, which is not a typical characteristic of human MASH. Subsequently, we performed liquid chromatography-mass spectrometry (LC-MS)-based metabolomic and lipidomic analyses to investigate the comprehensive metabolic alterations following the administration of KN21 (15 mg/kg), a direct AMPK activator selected based on its AMPK activation potency in our previous study [17], in a mouse model of MASH. Our findings demonstrate that KN21 treatment significantly ameliorated key pathological hallmarks of MASH, including hepatic steatosis and fibrosis. We propose that these therapeutic effects are strongly associated with alterations in long acyl chain glycerolipid metabolism and pyrimidine metabolism, suggesting a novel metabolic mechanism underlying AMPK-mediated hepatoprotection.

2. Materials and methods

2.1. Animals and treatments

Eight-week-old male C57BL/6 J mice were obtained from Raonbio (Gyonggi-do, South Korea). Following a one-week acclimatization period, the mice were randomly divided into four groups: (1) control group, which was fed a normal chow diet and treated with vehicle; (2) KN21 group, which was fed a normal chow diet and treated with KN21; (3) CDAHFD group, which was fed a choline-deficient, L-amino acid-defined high-fat diet (CDAHFD; 60 % fat, 0.1 % methionine; Research Diets Inc., #A06071302, NJ, USA) for six weeks; and (4) CDAHFD+KN21 group, which was fed a CDAHFD for six weeks and treated with KN21. KN21 was administered intraperitoneally at a dose of 15 mg/kg every 2 days for four weeks, starting from Week 2 of the CDAHFD feeding period. Before euthanasia, the mice were fasted for 12 h and then anesthetized with 2,2,2-tribromoethanol (Sigma—Aldrich, MO, USA).

Blood samples were collected from the inferior vena cava using a 1-mL syringe. After blood collection, the mice were euthanized by severing the inferior vena cava, followed by whole-body perfusion with phosphate-buffered saline (PBS) through the left ventricle. Livers were harvested, weighed, and processed as follows: the left lobe was promptly fixed in 10 % buffered formalin for histological evaluation, while the remaining liver tissues were rapidly frozen in liquid nitrogen and stored at –80 °C until further examination. All mice were housed in a temperature-controlled environment under a 12-h light/dark cycle with *ad libitum* access to food and water. Animal experiments were conducted in accordance with protocols approved by the Institutional Animal Care and Use Committee of Ewha Womans University (Approval No. 19–041) and adhered to the ARRIVE guidelines and the National Research Council's Guide for the Care and Use of Laboratory Animals.

2.2. In vivo western blot analysis

Western blot analysis was performed as previously described [15]. Briefly, liver tissues were lysed in HEPES buffer, and total protein extracts were obtained by centrifugation and quantified using a BCA protein assay kit (Thermo Fisher Scientific, MA, USA). Equal amounts of protein were separated via 10 % SDS-PAGE, transferred to PVDF membranes (Pall Life Sciences, NY, USA), and blocked with 5 % skim milk for 1 h at room temperature. The membranes were then incubated overnight at 4 °C with primary antibodies, followed by incubation with HRP-conjugated secondary antibodies. The protein bands were detected using an ECL reagent (GE Healthcare, IL, USA) and visualized with an LAS-3000 imaging system (Fuji Photo Film, Tokyo, Japan). Band intensities were analyzed via Multi Gauge Software (Fuji Photo Film) or Image Lab (Bio-Rad, CA, USA), and quantification was performed using ImageJ (NIH, MD, USA). The list of primary antibodies used is provided in Supplementary Table S1.

2.3. Histological examination of liver tissues

Histological analysis, including hematoxylin and eosin (H&E), sirius red, and immunohistochemical staining, was performed as previously described [16]. Briefly, formalin-fixed liver tissues were embedded in paraffin, sectioned into 5-μm slices, and stained with H&E and sirius red according to standard protocols. To perform the immunohistochemistry

(IHC) experiments, antigen retrieval was performed, followed by blocking and overnight incubation with primary antibodies at 4 °C. Detection was performed using a VECTASTAIN ABC kit (Vector Laboratories), and staining was visualized using 3,3′-diaminobenzidine (DAB) solution (Dako, Agilent, CA, USA) with Mayer's hematoxylin counterstaining. Images were acquired using an Axiophot 2 microscope (Carl Zeiss, Jena, Germany) at 200 × magnification, and quantification was performed using ImageJ software (NIH, MD, USA). The antibodies used for IHC are listed in Supplementary Table S1.

2.4. Quantitative real-time reverse-transcription PCR

A qRT-PCR assay was performed as described previously [16]. Briefly, total RNA was extracted from liver tissues using TRIzol reagent (FAVORGEN Biotech Corp., Kaohsiung, Taiwan). Real-time quantitative PCR (qRT-PCR) was performed using the SensiFAST™ SYBR No-ROX kit (Bioline, London, UK) according to the manufacturer's protocol. The relative expression levels of genes were determined using the ΔΔCt method and normalized to that of *GAPDH*. The sequences of primers used for qRT-PCR are provided in Supplementary Table S2.

2.5. Metabolomic and lipidomic analysis

Metabolomic and lipidomic analyses were performed using ultra-performance liquid chromatography- quadrupole time-of-flight mass spectrometry (UPLC-QTOF MS) at the Korea Basic Science Institute (Instrument Codes WS003, WS005 and WS007) as previously described [18]. Briefly, liver tissues (20 mg) were extracted using a methanol/water/chloroform biphasic method, and lipids of serum (20 μL) were extracted with a chloroform/methanol/water mixture. The aqueous and organic fractions obtained from liver and serum were dried and reconstituted in a water/acetonitrile mixture (1:1, v/v) and isopropanol for metabolomic and lipidomic analyses, respectively. The Quad LCMS QC reference material mix (P/N 186006963, Waters, MA, USA) and the Avanti Lipid SPLASH mix (P/N 330707, Avanti Polar Lipids Inc., AL, USA) were used as internal standards for metabolomic and lipidomic analyses, respectively.

Chromatographic separation of aqueous metabolites was achieved using an UPLC system (ACQUITY™ UPLC, Waters, Manchester, UK) on a ZIC-HILIC column (2.1 × 100 mm, 3.5 μm, Merck) coupled to a Triple TOF 5600 (Sciex, Concord, Canada) operating in both positive and negative electrospray ionization modes. Lipidomic profiling was conducted using an ACQUITY UPLC CSH C18 column (2.1 × 100 mm, 1.7 μm, Waters) connected to UPLC (ACQUITY™ UPLC, Waters, Manchester, UK) combined with a Xevo G2-XS QTOF-MS (Waters, MA, USA).

To ensure analytical consistency, pooled quality control (QC) samples were injected every six analytical runs, and features with coefficient of variation (CV) > 20 % in QC samples were excluded. Data processing was performed using MarkerView (Sciex) and Progenesis QI (Waters) for metabolomic and lipidomic datasets, respectively. Metabolite and lipid intensities were normalized to median fold change. Compound annotation was based on accurate mass, fragmentation pattern, and retention time matching against HMDB, METLIN, and in-house libraries. For further details, see the Supporting Information.

2.6. Statistical analysis

The data are presented as the means ± standard deviations (SDs). Statistical analyses were performed using GraphPad Prism 9.0 (GraphPad Software, Inc., CA, USA), SPSS software version 23.0 (SPSS Inc., IL, USA) and R software (version 4.2.2; R Core Team, Vienna, Austria). One-way analysis of variance (ANOVA) followed by Tukey's post hoc test was used to assess group differences in lipid and metabolite levels, biochemical parameters, and mRNA expression between groups. Pearson correlation coefficients were calculated using SPSS version 23.0 (SPSS Inc., IL, USA). To control for multiple hypothesis testing across all lipids and metabolites, p-values obtained from pairwise comparisons and Pearson correlation analyses were further adjusted using the Benjamini–Hochberg false discovery rate (FDR) correction. Statistical significance was defined as $p < 0.05$ or $q < 0.05$.

For the statistical analysis of the metabolomics and lipidomics data, after scaling to unit variance, partial least squares discriminant analysis (PLS-DA) was performed using SIMCA-P software (version 14.0, Umetrics, Umeå, Sweden). The reliability of the PLS-DA model was validated using a 100-repeated permutation test and a CV-ANOVA test.

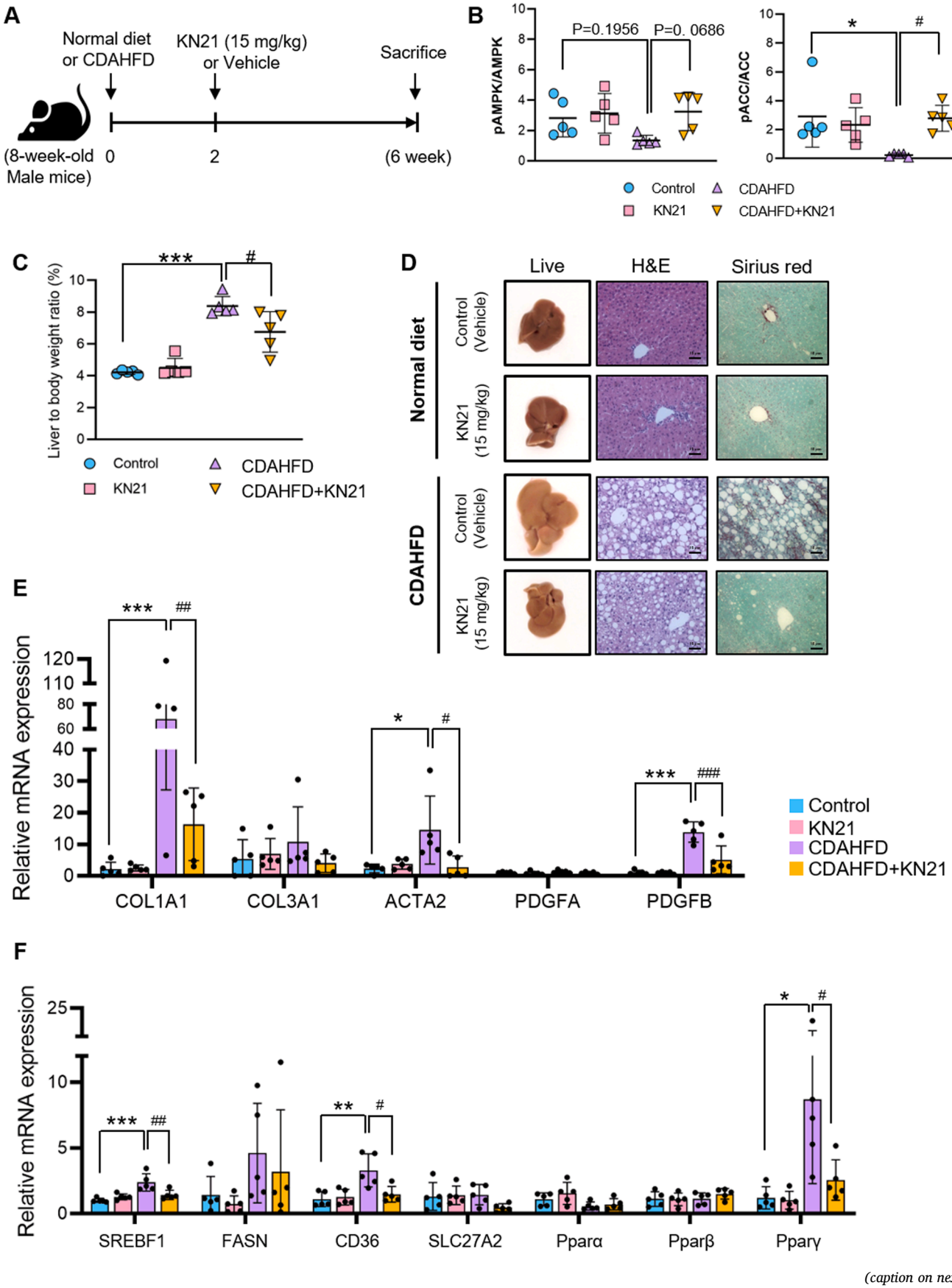
3. Results

3.1. AMPK activator KN21 alleviates hepatic steatosis and fibrosis

Eight-week-old male C57BL/6 J mice were fed either a normal diet or a CDAHFD for six weeks. KN21, a novel direct AMPK activator candidate, was administered intraperitoneally every two days for four weeks (total of 14 doses), starting at Week 2 (Fig. 1A). Compared with control mice fed a normal diet, CDAHFD-fed mice presented a significant reduction in AMPK phosphorylation, as indicated by the decreased p-AMPK/AMPK ratio and p-ACC/ACC ratio (Fig. 1B) and reduced p-AMPK and p-ACC expression (Figure S1A). However, KN21 treatment restored AMPK phosphorylation, confirming its ability to activate AMPK *in vivo*. Although there were no significant differences in body weight between the CDAHFD and CDAHFD+KN21 groups (Figure S1B), the liver-to-body weight ratio, a key indicator of hepatic steatosis, was significantly increased in CDAHFD-fed mice but significantly reduced following KN21 treatment (Fig. 1C). Histological analyses further confirmed the hepatoprotective effects of KN21. Hematoxylin and eosin (H&E) staining revealed alleviated hepatic steatosis, whereas sirius red staining revealed decreased collagen deposition, indicating reduced fibrosis in the CDAHFD+KN21 group (Figures 1D and S1D-E). Consistently, the mRNA expression levels of key fibrotic markers, including *COL1A1*, *ACTA2*, and *PDGFB*, which were significantly elevated in CDAHFD-fed mice, were markedly reduced following KN21 treatment (Fig. 1E). Additionally, qRT-PCR analysis of liver tissue was performed to evaluate changes in target genes such as *sterol regulatory element binding transcription factor 1 (SREBF1), cluster of differentiation 36 (CD36),* and *peroxisome proliferator-activated receptor-γ (PPARγ)*, which are associated with lipid metabolism and hepatic steatosis (Fig. 1F). The expression levels of *SREBF1*, *CD36*, and *PPARγ* were significantly increased in the CDAHFD group than in the control group. However, these increases were significantly attenuated in the CDAHFD+KN21 group (Fig. 1F). These findings suggest that KN21 effectively attenuates MASH progression by reducing hepatic steatosis, lipid accumulation and fibrosis. Regarding other key hallmarks of MASH, such as inflammation, our previous study showed that KN21 did not exert significant effects on these inflammatory parameters. Therefore, in the present study, we focused on steatosis and fibrosis, where KN21 exhibited the most pronounced effects.

3.2. AMPK activator KN21 reduces triglyceride levels and inhibits hepatic lipid accumulation in MASH mice

Hepatic lipid accumulation is a hallmark of MASH. To assess the impact of KN21 on lipid metabolism, lipidomic profiling was performed on liver samples from CDAHFD-fed mice and normal diet-fed controls. PLS-DA score plots revealed a distinct separation between the normal diet and CDAHFD groups along the PLS1 axis, indicating substantial lipidomic alterations in the liver following CDAHFD feeding (Fig. 2A). Interestingly, the CDAHFD+KN21 group was closer to that of the normal-diet control group, suggesting that KN21 treatment effectively modulates hepatic lipid metabolism (Fig. 2A). The robustness of the PLS-DA models was confirmed by permutation testing (Figure S2A). A total of 195 lipids were identified in both positive and negative ion modes using UPLC-QTOF MS (Table S3). Analysis of the percent distribution



(caption on next page)

Fig. 1. KN21 treatment ameliorates hepatic lipid accumulation and fibrosis in diet-induced MASH mice. (A) Schematic of the experimental design. Mice were fed a normal diet or a choline-deficient, L-amino acid-defined high-fat diet (CDAHFD) for six weeks to induce metabolic dysfunction-associated steatohepatitis (MASH). At Week 2, KN21 (15 mg/kg) or vehicle was administered intraperitoneally every 2 days for 4 weeks (14 doses in total). At Week 6, the mice were sacrificed, and their livers were harvested for analysis. (B) The ratio of phosphorylated AMPK (p-AMPK) to total AMPK and the ratio of phosphorylated ACC to total ACC in liver tissues with or without KN21 treatment. (C) Liver-to-body weight ratios of experimental mice in the control, KN21, CDAHFD, and CDAHFD+KN21 groups. (D) Representative liver tissue images from each experimental group stained with hematoxylin and eosin (H&E) and sirius red. (E) Relative mRNA expression levels of fibrosis markers, including *COL1A1*, *COL3A1*, *ACTA2*, *PDGFA*, and *PDGFB*, in liver tissues. (F) Relative mRNA expression levels of key genes involved in lipid metabolism, including *SREBP1*, *FASN*, *CD36*, *SLC27A2*, *PPARα*, *PPARβ*, and *PPARγ*, in liver tissues of mice from each treatment groups. The data are expressed as the means ± standard deviations for control mice (n = 5), KN21-treated mice (n = 5), CDAHFD mice (n = 5), and CDAHFD+KN21-treated mice (n = 5). One-way ANOVA followed by Tukey's post hoc test was used to evaluate significant differences between groups. *, ** and *** indicate $p < 0.05$, $p < 0.01$ and $p < 0.001$, respectively, for control vs. CDAHFD. $^{\#}$, $^{\#\#}$ and $^{\#\#\#}$ indicate $p < 0.05$, $p < 0.01$, and $p < 0.001$, respectively, for CDAHFD vs. CDAHFD+KN21.
AMPK, AMP-activated protein kinase; ACC, Acetyl-CoA Carboxylase; CDAHFD, choline-deficient, L-amino acid-defined high-fat diet; COL1A1, collagen type I alpha 1 chain; COL3A1, collagen type III alpha 1 chain; ACTA2, actin alpha 2; PDGFA, platelet-derived growth factor subunit A; PDGFB, platelet-derived growth factor subunit B; SREBF, sterol regulatory element-binding protein; CD36, cluster of differentiation 36; SLC27A2, solute carrier family 27 member 2; PPARα, peroxisome proliferator-activated receptor alpha; PPARβ, peroxisome proliferator-activated receptor beta; PPARγ, peroxisome proliferator-activated receptor gamma; FAS, fatty acid synthase.

derived from the total intensity of each lipid class revealed a significant reduction in phosphatidylcholine (PC), phosphatidylethanolamine (PE) and triacylglycerols with short-chain fatty acid (TAGs-SCFA) in CDAHFD-fed mice, whereas triacylglycerols with long-chain fatty acid (TAGs-LCFA) were significantly increased (Fig. 2B). Importantly, these lipidomic changes were partially reversed following KN21 treatment (Fig. 2B). To assess lipidomic alterations at the individual lipid species level, a heatmap plot was generated (Fig. 2C). Notably, DAG and TAGs-LCFA species were markedly increased in the CDAHFD group but restored to near-normal levels following KN21 treatment, whereas TAGs-SCFA remained unchanged (Fig. 2C). Next, bubble charts of the DAG and TAG species were generated to investigate the structural differences based on the number of double bonds and total carbon atoms (Fig. 2D). DAGs and TAGs containing long acyl chains (C52-C62) were significantly more abundant in the CDAHFD group than in the control group, but these levels were restored upon KN21 treatment (Fig. 2D). However, the levels of TAGs-SCFA did not recover to the levels of TAGs-LCFA after KN21 treatment (Fig. 2D). Similar lipidomic alterations were observed in the serum samples. PLS-DA score plots demonstrated partial separation between the CDAHFD and CDAHFD+KN21 groups, further supporting the systemic effects of KN21 (Figure S3A). Additionally, serum lipid heatmap analysis revealed a significant increase in the levels of TAGs-LCFA in the CDAHFD group, which was attenuated by KN21 administration, indicating its role in modulating systemic lipid metabolism in MASH (Figure S3C). Collectively, these findings suggest that the AMPK activation induced by KN21 treatment alleviates disrupted hepatic and systemic lipid metabolism in a mouse model of MASH, highlighting its potential therapeutic efficacy in restoring lipid homeostasis.

3.3. AMPK activator KN21 induces alterations in pyrimidine metabolism in MASH mice

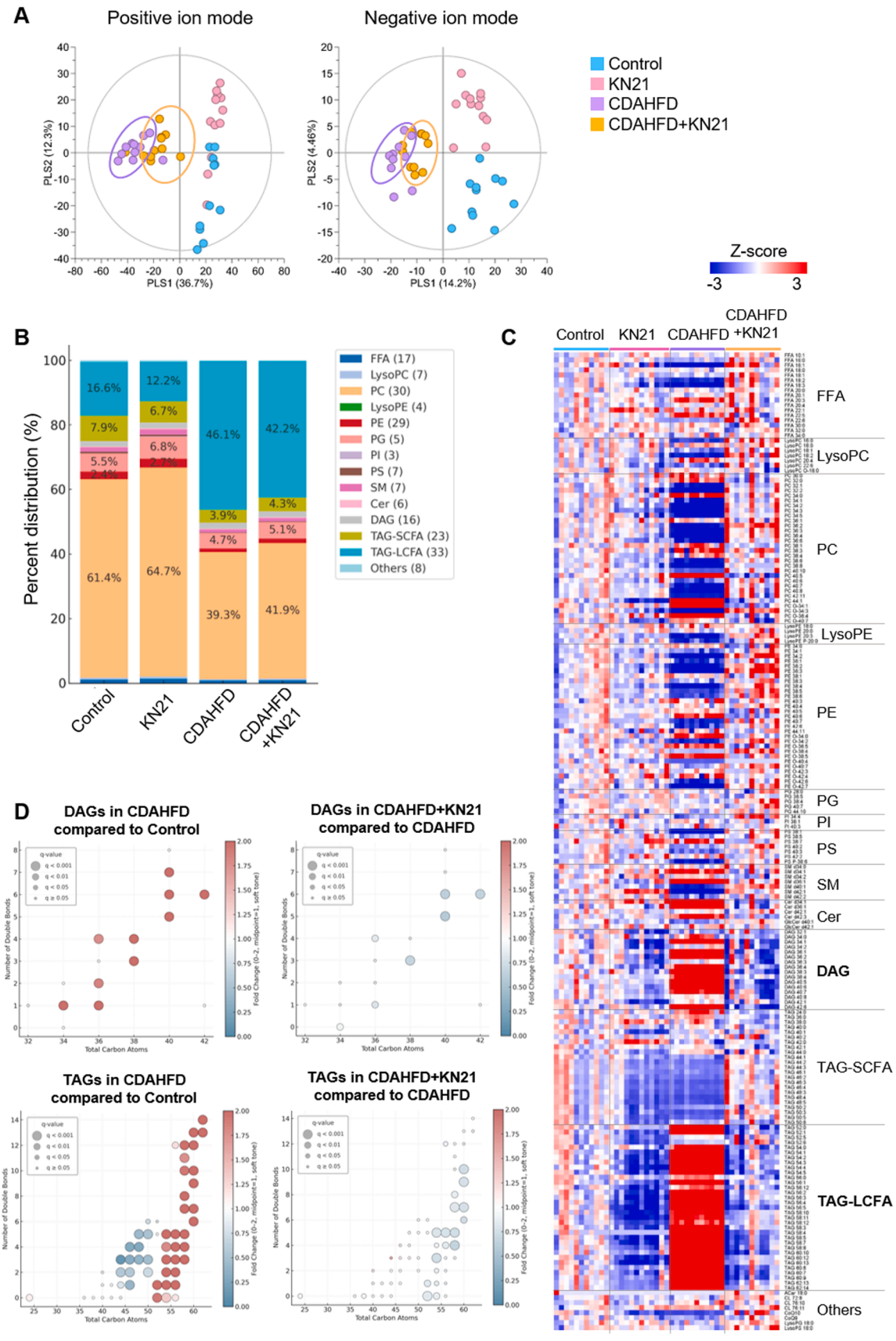
In addition to its role in lipid metabolism, AMPK regulates key metabolic pathways, including energy, amino acid, and nucleotide metabolism [10,11]. To explore the metabolic alterations induced by KN21 in the MASH mouse model, untargeted metabolomic profiling was performed using UPLC-QTOF MS. Multivariate analysis revealed distinct clustering patterns based on diet type and KN21 treatment, as shown in the PLS-DA score plot in positive ion mode, indicating that both CDAHFD and AMPK activation led to significant metabolic alterations in the liver (Fig. 3A). The robustness of the PLS-DA model was confirmed by a permutation test (Figure S2B). A total of 87 aqueous metabolites, such as amino acids, nucleotides, vitamins, carbohydrates, and acylcarnitines, were identified in both positive and negative ion modes (Table S4). Among these, the levels of 52 metabolites were significantly different between the control and CDAHFD groups. Notably, the levels of only glycerophosphocholine and uridine were significantly restored in liver tissues following KN21 treatment (Fig. 3B and Table S4). The key metabolites involved in pyrimidine metabolism, including cytidine, cytidine monophosphate (CMP), cytosine, uracil, uridine and uridine 5-diphosphate (UDP), were significantly altered in the CDAHFD group compared with the control group but were recovered following KN21 treatment (Fig. 3C). These findings demonstrate that KN21 treatment alleviates metabolic abnormalities in MASH by restoring pyrimidine metabolism, particularly uracil and uridine metabolism.

3.4. AMPK activation inhibits lipid accumulation and fibrosis associated with hepatic metabolism

The expression of SREBP1 (encoded by *SREBF1*), a transcription factor for fatty acid synthesis, is known to upregulate CD36, which is located on the surface of cells and facilitates the uptake of LCFAs [19]. PPARγ functions as a transcription factor, regulating the expression of genes involved in various processes, including adipocyte differentiation, insulin sensitivity, and fatty acid metabolism, and plays a crucial role in lipid storage and utilization [19]. Therefore, to further investigate the relationships between key metabolites and molecular markers of hepatic steatosis and fibrosis, Pearson correlation analysis was performed. Uridine and uracil levels were negatively correlated with the expression of *COL1A1*, *PDGFB*, *SREBF1*, and *CD36* suggesting that disruptions in pyrimidine metabolism are associated with increased fibrosis severity and lipid accumulation (Fig. 4A). In contrast, the abundance of TAGs with long acyl chain showed a significant positive correlation with the expression of *COL1A1*, *PDGFB*, *SREBF1*, *CD36*, and *PPARγ* but a negative, though not statistically significant, correlation with *PPARα* expression, a key regulator of fatty acid oxidation (FAO) [20] (Fig. 4A). These findings suggest that AMPK activation by KN21 plays a pivotal role in restoring metabolic homeostasis, attenuating hepatic lipid accumulation, and alleviating fibrosis in a mouse model of MASH (Fig. 4B).

4. Discussion and conclusion

AMPK activation has emerged as a potential therapeutic strategy for MASH due to its critical role in regulating hepatic lipid metabolism, reducing inflammation, and mitigating fibrosis and liver injury [10,21]. In diet-induced MASH mouse models, AMPK activation has been shown to protect hepatocytes from apoptosis by primarily inhibiting pro-caspase 6 phosphorylation and caspase 6 activity [22]. As a central regulator of energy homeostasis, AMPK modulates key metabolic processes, including DNL and FAO, and mitochondrial function. Its activation suppresses key lipogenic enzymes such as fatty acid synthase (FAS) and acetyl-CoA carboxylase (ACC) while enhancing lipid oxidation, thereby reducing hepatic steatosis and metabolic dysfunction [23,24]. However, despite its therapeutic potential, the development of AMPK activators for MASH treatment has been limited by an incomplete understanding of the metabolic reprogramming associated with AMPK



(caption on next page)

Fig. 2. KN21 treatment alters lipid metabolism in diet-induced MASH mice. (A) Partial least squares-discriminant analysis (PLS-DA) score plots derived from UPLC-QTOF MS spectra of global hepatic lipid profiles in positive ion mode ($R^2X = 76.8$ %, $R^2Y = 98.4$ %, $Q^2 = 80.2$ %) and negative ion mode ($R^2X = 18.6$ %, $R^2Y = 54.5$ %, $Q^2 = 20.8$ %). (B) Percentage distributions of lipid classes in liver tissues from each experimental group. (C) Heatmap of lipid species in liver tissues from the control, KN21, CDAHFD, and CDAHFD+KN21 groups. The heatmap was color-coded based on the z score of the relative intensities of each lipid species. (D) Bubble charts of diacylglycerol (DAG) and triacylglycerol (TAG) species. Each filled circle represents an individual lipid species, plotted based on the total number of carbon atoms (x-axis) and double bonds (y-axis). The color intensity reflects the magnitude of the fold change, and the circle radius indicates the significance level (q value). The levels of lipids were derive from the control mice (n = 11), KN21-treated mice (n = 12), CDAHFD mice (n = 11), and CDAHFD+KN21-treated mice (n = 11). One-way ANOVA followed by Tukey's post hoc test was performed, and the resulting p-values were adjusted for multiple testing using the Benjamini–Hochberg false discovery rate (FDR) correction ($q < 0.05$ was considered statistically significant) to evaluate significant differences between groups.
CDAHFD, choline-deficient, L-amino acid-defined high-fat diet; FFA, free fatty acid; LysoPC, lysophosphatidylcholine; PC, phosphatidylcholine; LysoPE, lysophosphatidylethanolamine; PE, phosphatidylethanolamine; PG, phosphatidylglycerol; PI, phosphatidylinositol; PS, phosphatidylserine; SM, sphingomyelin; Cer, ceramide; DAG, diacylglycerol; TAG, triacylglycerol; TAGs-SCFA, triacylglycerols with short-chain fatty acid; TAGs-LCFA, triacylglycerols with long-chain fatty acid.

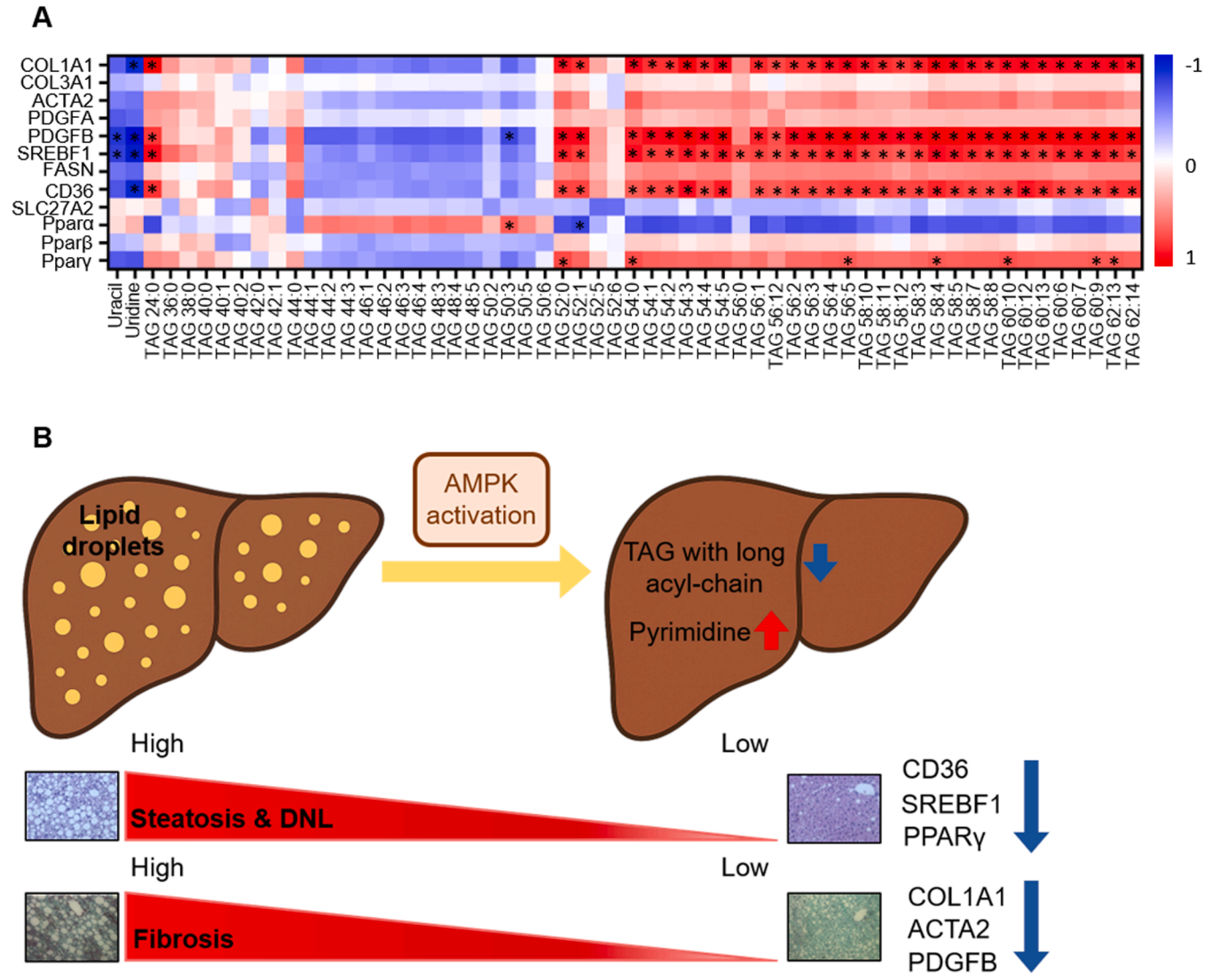
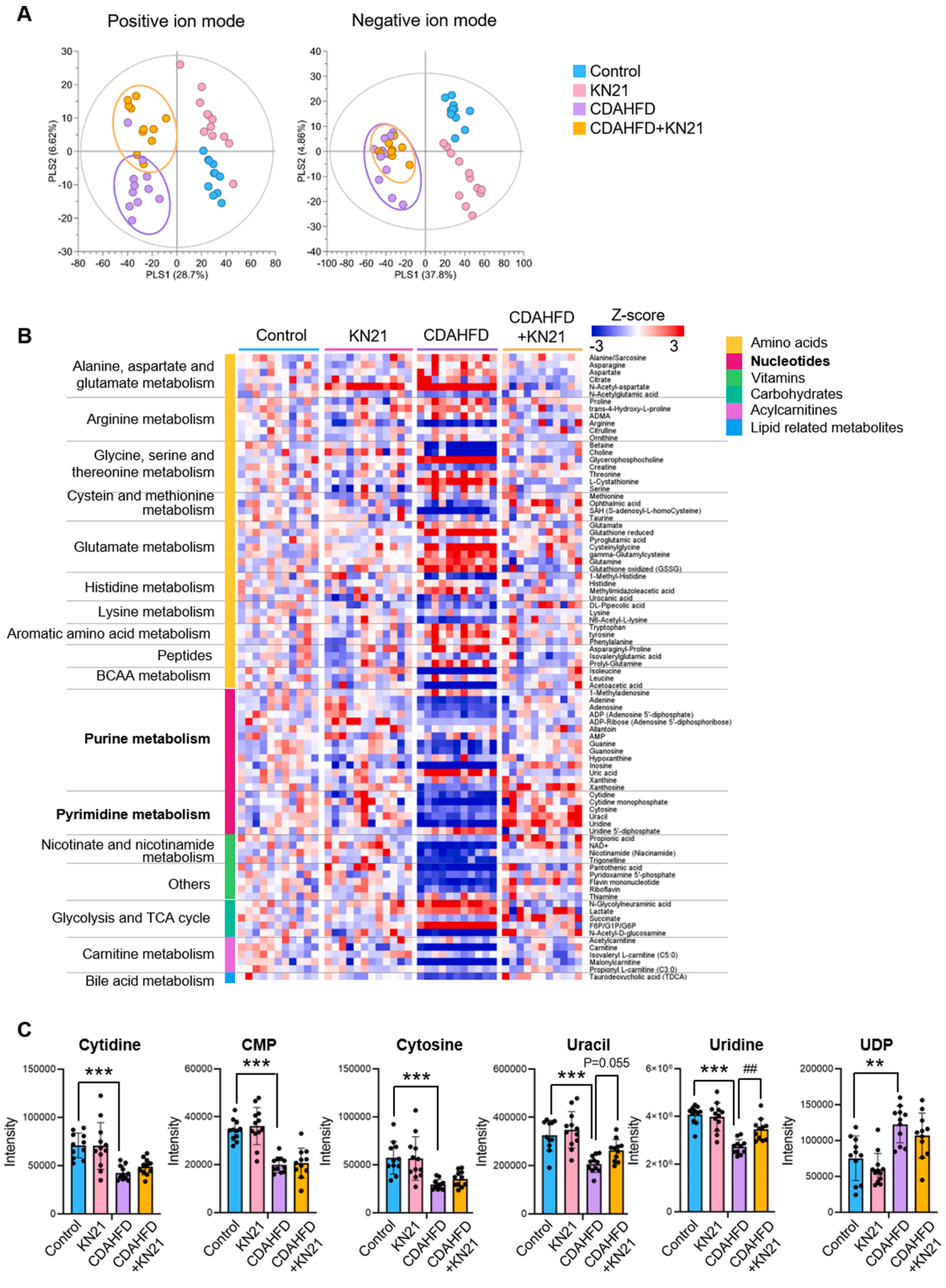


Fig. 3. KN21 treatment alters hepatic metabolism in diet-induced MASH mice. (A) PLS-DA score plots derived from UPLC-QTOF MS spectra of global hepatic metabolic profiles in positive ion mode ($R^2X = 35.3$ %, $R^2Y = 50.9$ %, $Q^2 = 31.8$ %) and negative ion mode ($R^2X = 51.1$ %, $R^2Y = 84.8$ %, $Q^2 = 47.9$ %). (B) Heatmap of metabolites in the liver tissues of each experimental group, curated according to their respective KEGG pathways. The heatmap was color-coded based on the z score of the relative intensity of each metabolite. (C) Alterations in the levels of key metabolites involved in pyrimidine metabolism. The data are expressed as the means ± standard deviations. The levels of metabolites were derive from the control mice (n = 11), KN21-treated mice (n = 12), CDAHFD mice (n = 11), and CDAHFD+KN21-treated mice (n = 11). One-way ANOVA followed by Tukey's post hoc test was performed, and the resulting p-values were adjusted for multiple testing using the Benjamini–Hochberg false discovery rate (FDR) correction ($q < 0.05$ was considered statistically significant) to evaluate significant differences between groups. *, ** and *** indicate $q < 0.05$, $q < 0.01$, and $q < 0.001$, respectively, for control vs. CDAHFD. #, ## and ### indicate $q < 0.05$, $q < 0.01$ and $q < 0.001$, respectively, for CDAHFD vs. CDAHFD+KN21.
CDAHFD, choline-deficient, L-amino acid-defined high-fat diet; CMP, cytidine monophosphate; UDP, uridine 5-diphosphate.



(caption on next page)

Fig. 4. Effects of KN21 on liver metabolism-associated gene expression, steatosis, and fibrosis in MASH mice. (A) Pearson's correlation analysis was performed between pyrimidine metabolites, TAG species, and markers of steatosis and fibrosis in control mice (n = 5), KN21-treaged mice (n = 5), CDAHFD mice (n = 5), and CDAHFD+KN21-treated mice (n = 5). The resulting p-values were adjusted for multiple testing using the Benjamini–Hochberg false discovery rate (FDR) correction (q < 0.05 was considered statistically significant). Red and blue indicate positive and negative correlations, respectively (*q < 0.05). (B) Schematic summary illustrating the effects of AMPK activation by KN21 on ameliorating hepatic steatosis, de novo lipogenesis (DNL), and fibrosis by reprogramming hepatic lipid and pyrimidine metabolism.

AMPK, AMP-activated protein kinase; CDAHFD, choline-deficient, L-amino acid-defined high-fat diet; COL1A1, collagen type I alpha 1 chain; COL3A1, collagen type III alpha 1 chain; ACTA2, actin alpha 2; PDGFA, platelet-derived growth factor subunit A; PDGFB, platelet-derived growth factor subunit B; SREBF, sterol regulatory element-binding protein; CD36, cluster of differentiation 36; SLC27A2, solute carrier family 27 member 2; PPARα, peroxisome proliferator-activated receptor alpha; PPARβ, peroxisome proliferator-activated receptor beta; PPARγ, peroxisome proliferator-activated receptor gamma; FAS, fatty acid synthase; de novo lipogenesis (DNL); TAG, triacylglycerol; TAGs-SCFA, triacylglycerols with short-chain fatty acid; TAGs-LCFA, triacylglycerols with long-chain fatty acid.

activation. In this study, we investigated the effects of KN21, reported as a direct AMPK activator [17], using UPLC-QTOF MS-based metabolomics and lipidomics approaches in a diet-induced MASH mouse model. Our findings demonstrate that KN21 effectively alleviates hepatic steatosis and fibrosis, and restores the alterations in long-chain acyl TAG and pyrimidine metabolism. Ultimately, these effects were strongly associated with each other, suggesting a coordinated metabolic response regulated by AMPK activation.

The liver is central to lipid metabolism, where excess fatty acids are taken up and incorporated into TAG pools. Chronic dysregulation of this process leads to hepatic lipotoxicity, inflammation, and fibrosis—hallmarks of MASH [25]. Lipidomic analyses have revealed a significant accumulation of TAGs, particularly those with LCFAs, in both the blood and liver tissues of patients with metabolic diseases such as obesity, fatty liver disease, and MASH. Long-chain TAGs have been proposed as potential biomarkers for predicting disease onset and the severity of hepatic steatosis [26–28]. In this study, TAGs-LCFAs (C52-C62) were significantly elevated in the CDAHFD group, whereas a marked reduction in these lipid species was observed following KN21 treatment. These findings underscore the importance of regulating TAG metabolism to alleviate hepatic lipid accumulation and prevent the progression of fatty liver disease, highlighting the potential of AMPK activation as a therapeutic approach for MASH. A previous study suggested that *Boesenbergia pandurate* extract (BPE) inhibits TAG accumulation, obesity, and fatty liver in high-fat diet (HFD)-induced obesity in mice, as well as in 3T3-L1 adipocytes and HepG2 hepatocytes, through AMPK activation and the regulation of lipid metabolism-related proteins, including ACC, FAS, SREBP-1c, and PPARγ [29]. Consistently, our results demonstrated that the expression levels of CD36, SREBF1 and PPARγ were significantly increased in CDAHFD-fed mice but markedly reduced following KN21 treatment, suggesting that KN21 attenuates hepatic lipid accumulation and lipotoxicity in the MASH mouse model by inhibiting fatty acid uptake, *de novo* fatty acid synthesis, and TAG biosynthesis.

CD36, a fatty acid translocase, plays a crucial role in the uptake and intracellular transfer of very long-chain fatty acids (VLCFAs) [30]. CD36 overexpression has been implicated in the pathogenesis of MASH [31]. Previous studies have demonstrated that CD36 knockout mice exhibit reduced fatty acid uptake and TAG levels, underscoring the role of CD36 in hepatic lipid accumulation [32]. Additionally, SREBP1, a master transcription factor for fatty acid synthesis, regulates the expression of CD36, thereby promoting long-chain fatty acid uptake into cells and further promoting fatty acid synthesis [33,34]. Recent studies have also suggested that CD36 can influence SREBP activity through the formation of complexes with insulin-induced gene-2 (INSIG2), disrupting the interaction between SREBP cleavage-activating protein and INSIG2 and leading to the translocation of SREBP1 from the endoplasmic reticulum to the Golgi and further promoting lipogenesis [35]. Both SREBP1 and CD36 work in concert to maintain energy homeostasis, ensuring a balance between fatty acid synthesis and utilization. Their upregulation has been observed in MASH patients, suggesting that excessive DNL, exacerbated by CD36-mediated LCFA uptake, contributes to lipid overload and lipotoxicity in hepatocytes [26,35,36]. In our study, KN21 treatment restored SREBP1 and CD36 expression to near-normal levels, indicating that AMPK activation suppresses both DNL and LCFA uptake, thereby mitigating hepatic lipid accumulation.

Peroxisome proliferator-activated receptors (PPARs) are key regulators of lipid metabolism, particularly in the transcriptional control of enzymes involved in very long-chain fatty acid (VLCFA) metabolism [37]. PPARα is a major transcription factor that promotes FAO, whereas PPARγ primarily facilitates lipid storage and adipogenesis [38,39]. In the liver, excessive dietary lipid intake suppresses PPARα expression while upregulating PPARγ, leading to hepatic lipid accumulation. This shift occurs because PPARγ upregulation enhances SREBP-1c activity, which in turn suppresses carnitine palmitoyltransferase-1 (CPT-1), a key PPARα target gene required for mitochondrial FAO, further promoting TAG accumulation and exacerbating hepatic steatosis [40,41]. Our study revealed that KN21 administration downregulated PPARγ expression, supporting the hypothesis that AMPK activation restores hepatic lipid homeostasis by balancing PPAR signaling.

In addition to its lipid-lowering effects, KN21 also demonstrated significant antifibrotic properties in this study. The expression of key fibrosis markers, including *COL1A1*, *ACTA2* (encoding α-SMA), and *PDGFB*, was significantly elevated in MASH mouse livers but was markedly reduced following KN21 treatment. This reduction in fibrosis markers was further supported by Pearson correlation analysis, which revealed a positive correlation between these markers and TAG accumulation and a negative correlation with pyrimidine metabolites. These findings suggest that the antifibrotic effects of KN21 may be mediated, in part, by its ability to restore lipid homeostasis and pyrimidine metabolism. Hepatic fibrosis in MASH is driven primarily by the activation of hepatic stellate cells (HSCs), which undergo a phenotypic transition into myofibroblast-like cells characterized by increased extracellular matrix (ECM) deposition and excessive collagen production [42]. This fibrogenic process is fueled by extensive metabolic reprogramming, including enhanced glycolysis, TCA cycle activity, and lipid metabolism, providing the substantial energy required for ECM synthesis and cell proliferation [43]. Notably, previous studies have reported that inhibiting DNL through ACC and FASN inhibitors reduces collagen formation by downregulating fibrosis-associated genes, including *COL1A1*, *COL3A1*, and *ACTA2*, a hallmark of activated HSCs [44,45]. These findings align with our observation that KN21 treatment, which activates AMPK, significantly reduces the expression of COL1A1 and α-SMA in MASH mouse livers. Furthermore, recent studies have highlighted the critical role of saturated lipid accumulation in fibrosis progression. Jia et al. utilized multimodal nonlinear optical microscopy to examine unsaturated TAG accumulation in a CCl_4-induced liver fibrosis model. Their study revealed a progressive increase in unsaturated TAG levels in late-stage fibrosis, accompanied by reduced membrane fluidity and decreased lipid unsaturation [46]. This imbalance in lipid accumulation contributes to ECM stiffening and further activation of HSCs, promoting fibrosis. Consistently, our findings demonstrated that the elevated TAG levels in MASH livers, which are composed predominantly of long acyl chains and unsaturated TAGs, were significantly reduced following KN21 treatment, suggesting that AMPK activation can effectively restore lipid homeostasis and potentially alleviate fibrosis.

Pyrimidine metabolism plays a crucial role in lipid homeostasis in the liver [47]. Uridine, a key metabolite in this pathway, is synthesized primarily in the liver and is essential not only for nucleoside synthesis

but also for regulating lipid metabolism. Uridine is degraded into uracil by uridine phosphorylase 1 (UPase1), which is encoded by the UPP1 (Uridine Phosphorylase 1) gene, and inhibition of this enzyme has been shown to increase hepatic uridine levels [48]. Elevated UPase1 expression has been linked to hepatic steatosis in mice, highlighting its potential role in lipid dysregulation and MASH progression [49]. Several studies have demonstrated that manipulating pyrimidine metabolism can significantly impact hepatic lipid accumulation and fibrosis. For example, Sullivan et al. reported that the inhibition of dihydropyrimidine dehydrogenase (DPYD), the rate-limiting enzyme in uridine catabolism, by the small-molecule DPYD inhibitor gimeracil reduced lipogenesis and enhanced mitochondrial FAO in hepatocytes [50]. Furthermore, direct uridine supplementation in obese mice reduced hepatic lipid accumulation and altered the gut microbiota composition by lowering the Firmicutes-to-Bacteroidetes ratio, suggesting a potential role for uridine in preventing obesity-related liver disease [51]. Additionally, inhibition of UPase1 activity using potassium 5-cyano-4-methyl-6-oxo-1,6-dihydropyridine-2-olate or direct uridine injection in CCl_4-induced fibrotic mice significantly alleviated both liver fibrosis and liver injury [52,53]. Furthermore, accumulating studies suggest that AMPK regulates nucleotide metabolism through indirect but biologically meaningful mechanisms. For example, AMPK serves as a central metabolic sensor that can coordinate cellular energy status with nucleotide metabolism. Activation of AMPK inhibits de novo pyrimidine synthesis via the mTORC1–CAD axis, as suppression of mTORC1 leads to the inhibition of CAD (carbamoyl phosphate synthetase 2/aspartate transcarbamylase/dihydroorotase), a multifunctional enzyme complex responsible for catalyzing the first, rate-limiting steps of pyrimidine biosynthesis [54]. This pathway provides a direct link between cellular energy availability and the regulation of pyrimidine production. In addition, ATP depletion has been shown to increase uridine concentrations by inducing pyrimidine degradation and promoting adenine nucleotide catabolism, which elevates purine base levels and consequently enhances uridine accumulation [55]. Therefore, through its ability to sense and modulate intracellular ATP levels and mTORC1-CAD axis, AMPK may indirectly influence pyrimidine metabolism, including the regulation of uridine homeostasis. These findings collectively highlight the critical role of pyrimidine metabolism in regulating lipid homeostasis and fibrosis progression. In our study, MASH mice presented significantly reduced hepatic levels of uridine and uracil, likely reflecting their increased utilization for DNL and pyrimidine catabolism, a pathway closely linked to acetyl-CoA metabolism. However, KN21 treatment restored these pyrimidine metabolite levels, suggesting that AMPK activation can rebalance pyrimidine metabolism, thereby mitigating lipid accumulation and fibrosis.

This study demonstrated that MASH is associated with significant dysregulation of long-chain acyl TAG and pyrimidine metabolism, which may in turn contribute to hepatic steatosis and fibrosis. Treatment with KN21, a novel direct AMPK activator, effectively ameliorated these metabolic abnormalities, highlighting the therapeutic potential of AMPK activation in MASH. Given the critical role of long-chain acyl TAGs and pyrimidine metabolism in MASH pathogenesis, targeting these pathways through AMPK activation may represent a promising therapeutic strategy. Future studies should focus on comparative analyses of AMPK activators to assess potential differences in metabolic reprogramming and therapeutic efficacy. All experiments in this study were conducted using male mice. Given that sex-dependent differences exist in metabolic regulation and inflammatory responses, future studies including female mice are warranted to validate the generalizability of our findings. Furthermore, integrating metabolomics and lipidomics approaches will further elucidate the precise molecular mechanisms underlying AMPK-mediated metabolic modulation in MASH, ultimately facilitating the development of more effective pharmacological interventions.

CRediT authorship contribution statement

Jueun Lee: Writing – original draft, Methodology, Investigation, Data curation, Formal analysis. **Seojeong Kim:** Writing – original draft, Methodology, Investigation, Data curation, Formal analysis. **Yeajin Ju:** Writing – original draft, Methodology, Investigation, Formal analysis. Minjung Seo: Methodology, Formal analysis. **Hyeri Kim:** Methodology, Formal analysis. **Jae-Ho Shin:** Methodology, Formal analysis. **Younghwa Na:** Methodology, Formal analysis. **Youngjoo Kwon:** Writing – review & editing, Supervision, Conceptualization, Funding acquisition. **Geum-Sook Hwang:** Writing – review & editing, Supervision, Conceptualization, Funding acquisition.

Declaration of Competing Interest

The authors declare that they have no known competing financial interests or personal relationships that could have appeared to influence the work reported in this paper.

Acknowledgments

This research was supported by the Basic Science Research Program through the National Research Foundation of Korea (NRF), funded by the Korean government (MSIT) (NRF-RS-2024–00345936, NRF-2022R1A2C2092053, RS-2024–00431505) and funded by the Ministry of Education (2021R1A6C101A442). Additionally, this research received support from the Korea Basic Science Institute (No. C523100 and No. C523400). The authors gratefully acknowledge the technical support provided by the Ewha Drug Development Research Core Center for qRT-PCR, NMR, and histochemical analyses.

Appendix A. Supporting information

Supplementary data associated with this article can be found in the online version at doi:10.1016/j.biopha.2025.118798.

Data availability

Data will be made available on request.

References

[1] E.E. Powell, V.W.-S. Wong, M.J.T.L. Rinella, Non-alcoholic fatty liver disease, Lancet 397 (10290) (2021) 2212–2224.
[2] J.M. Fraile, S. Palliyil, C. Barelle, A.J. Porter, M.J.Dd Kovaleva, development, therapy, Non-alcoholic steatohepatitis (NASH)–A review of a crowded clinical landscape, driven by a complex disease, Drug Des. Dev. Ther. (2021) 3997–4009.
[3] D. Ferguson, B.N. Finck, Emerging therapeutic approaches for the treatment of NAFLD and type 2 diabetes mellitus, Nat. Rev. Endocrinol. 17 (8) (2021) 484–495.
[4] S. Raza, S. Rajak, A. Upadhyay, A. Tewari, R.A.J.Fib Sinha, Current treatment paradigms and emerging therapies for NAFLD/NASH, Front. Biosci. 26 (2021) 206.
[5] E. Roeb, A.J.Zf.G. Geier, Nonalcoholic steatohepatitis (NASH)–current treatment recommendations and future developments, Gastroenterologie 57 (04) (2019) 508–517.
[6] R. Vuppalanchi, M. Noureddin, N. Alkhouri, A.J. Sanyal, Hepatology, therapeutic pipeline in nonalcoholic steatohepatitis, Nat. Rev. Gastroenterol. Hepatol. 18 (6) (2021) 373–392.
[7] S.J.J.D. Keam, Resmetirom: first approval, Drugs 84 (6) (2024) 729–735.
[8] D.J.Coicb Carling, AMPK signalling in health and disease, Curr. Opin. Cell Biol. 45 (2017) 31–37.
[9] P.J.N.R.M.C.B. Strzyz, AMPK against NASH, Nat. Rev. Mol. Cell Biol. 21 (4) (2020), 181–181.
[10] H. An, Y. Jang, J. Choi, J. Hur, S. Kim, Y.J.B. Kwon, Therapeutics, new insights into AMPK, as a potential therapeutic target in metabolic dysfunction-associated steatotic liver disease and hepatic fibrosis, Biomol. Ther. 33 (1) (2024) 18.
[11] B.K. Smith, K. Marcinko, E.M. Desjardins, J.S. Lally, R.J. Ford, G.R. Steinberg, Treatment of nonalcoholic fatty liver disease: role of AMPK, Am. J. Physiol. Endocrinol. Metab. 311 (4) (2016) E730–E740.
[12] H. Yang, D.H. Suh, D.H. Kim, E.S. Jung, K.H. Liu, C.H. Lee, C.Y.J.Bjop Park, Metabolomic and lipidomic analysis of the effect of pioglitazone on hepatic steatosis in a rat model of obese type 2 diabetes, Br. J. Pharmacol. 175 (17) (2018) 3610–3625.

[13] S.M. Lee, J. Lee, E. Kang, H.-L. Kim, G.-S. Hwang, J.J.P. Jung, Lipidomic analysis reveals therapeutic effects of Yijin-Tang on high-fat/high-cholesterol diet-induced obese mice, Phytomedicine 74 (2020) 152936.
[14] L.B. Avery, N.N.J.Mp Bumpus, Valproic acid is a novel activator of AMP-activated protein kinase and decreases liver mass, hepatic fat accumulation, and serum glucose in obese mice, Mol. Pharmacol. 85 (1) (2014) 1–10.
[15] J. Shinn, S. Park, S. Lee, N. Park, S. Kim, S. Hwang, J.J. Moon, Y. Kwon, Y. Lee, Antioxidative hyaluronic acid–bilirubin nanomedicine targeting activated hepatic stellate cells for anti-hepatic-fibrosis therapy, ACS Nano 18 (6) (2024) 4704–4716.
[16] S. Park, S. Hwang, J. Sun, K.-H. Jeon, N. Sheen, S. Shin, T.H. Kim, Y.-S. Lee, W. Seo, J.-S. Ryu, A novel A2a adenosine receptor inhibitor effectively mitigates hepatic fibrosis in a metabolic dysfunction-associated steatohepatitis mouse model, Int. J. Biol. Sci. 20 (5) (2024) 1855.
[17] S. Kim, J.-H. Shin, M. Seo, E.S. Pak, K.-H. Jeon, I. Moon, J. Kang, W. Seo, Y. Na, Y. Kwon, Pharmacological activation of AMP-activated protein kinase ameliorates liver fibrosis in a metabolic dysfunction-associated steatohepatitis mouse model, Int. J. Biol. Sci. 21 (7) (2025) 2957–2972.
[18] S. Lee, J. Lee, K.-S. Lyoo, Y. Shin, D.-M. Shin, J.-W. Kim, J.-S. Yang, K.-C. Kim, J.-Y. Lee, G.-S. Hwang, Unraveling metabolic signatures in SARS-CoV-2 variant infections using multiomics analysis, Front. Immunol. 15 (2024) 1473895.
[19] T. Varga, Z. Czimmerer, L. Nagy, PPARs are a unique set of fatty acid regulated transcription factors controlling both lipid metabolism and inflammation, Biochim. Et. Biophys. Acta (BBA) Mol. Basis Dis. 1812 (8) (2011) 1007–1022.
[20] L. Yao, B. Cao, Q. Cheng, W. Cai, C. Ye, J. Liang, W. Liu, L. Tan, M. Yan, B. Li, L. Physiology, Inhibition of soluble epoxide hydrolase ameliorates hyperhomocysteinemia-induced hepatic steatosis by enhancing β-oxidation of fatty acid in mice, Gastrointest. Liver Physiol. 316 (4) (2019) G527–G538.
[21] P. Zhao, A.R. Saltiel, From overnutrition to liver injury: AMP-activated protein kinase in nonalcoholic fatty liver diseases, J. Biol. Chem. 295 (34) (2020) 12279–12289.
[22] P. Zhao, X. Sun, C. Chaggan, Z. Liao, K. In Wong, F. He, S. Singh, R. Loomba, M. Karin, J.L.J.S. Witztum, An AMPK–caspase-6 axis controls liver damage in nonalcoholic steatohepatitis, Science 367 (6478) (2020) 652–660.
[23] D.J.Ijoo Hardie, AMPK: a key regulator of energy balance in the single cell and the whole organism, Int. J. Obes. 32 (4) (2008) S7–S12.
[24] N. Ouchi, R. Shibata, K.J.Cr Walsh, AMP-activated protein kinase signaling stimulates VEGF expression and angiogenesis in skeletal muscle, Circ. Res. 96 (8) (2005) 838–846.
[25] D.H. Ipsen, J. Lykkesfeldt, P. Tveden-Nyborg, Molecular mechanisms of hepatic lipid accumulation in non-alcoholic fatty liver disease, Cell Mol. Life Sci. 75 (18) (2018) 3313–3327.
[26] F. Chiappini, A. Coilly, H. Kadar, P. Gual, A. Tran, C. Desterke, D. Samuel, J.-C. Duclos-Vallée, D. Touboul, J.J.Sr Bertrand-Michel, Metabolism dysregulation induces a specific lipid signature of nonalcoholic steatohepatitis in patients, Sci. Rep. 7 (1) (2017) 46658.
[27] C. Peng, F. Chiappini, S. Kaščáková, M. Danulot, C. Sandt, D. Samuel, P. Dumas, C. Guettier, F.J.A. Le Naour, Vibrational signatures to discriminate liver steatosis grades, Analyst 140 (4) (2015) 1107–1118.
[28] X. Yin, C. Willinger, J. Keefe, J. Liu, A. Fernandez-Ortiz, B. Ibanez, J. Penalvo, A. Adourian, G. Chen, D. Corella, Lipidomic profiling identifies signatures of metabolic risk, eBioMedicine 51 (2020) 102520.
[29] D.-Y. Kim, M.-S. Kim, B.-K. Sa, M.-B. Kim, J.-K.J.Ijoms Hwang, Boesenbergia pandurata attenuates diet-induced obesity by activating AMP-activated protein kinase and regulating lipid metabolism, Int. J. Mol. Sci. 13 (1) (2012) 994–1005.
[30] V.A. Drover, D.V. Nguyen, C.C. Bastie, Y.F. Darlington, N.A. Abumrad, J.E. Pessin, E. London, D. Sahoo, M.C. Phillips, CD36 mediates both cellular uptake of very long chain fatty acids and their intestinal absorption in mice, J. Biol. Chem. 283 (19) (2008) 13108–13115.
[31] P. Rada, Á. González-Rodríguez, C. García-Monzón, Á.M.J.Cd Valverde, Disease, understanding lipotoxicity in NAFLD pathogenesis: is CD36 a key driver? Cell Death Dis. 11 (9) (2020) 802.
[32] C.G. Wilson, J.L. Tran, D.M. Erion, N.B. Vera, M. Febbraio, E.J.J.E. Weiss, Hepatocyte-specific disruption of CD36 attenuates fatty liver and improves insulin sensitivity in HFD-fed mice, Endocrinology 157 (2) (2016) 570–585.
[33] D. Eberlé, B. Hegarty, P. Bossard, P. Ferré, F.J.B. Foufelle, SREBP transcription factors: master regulators of lipid homeostasis, Biochimie 86 (11) (2004) 839–848.
[34] S.J.Er Kersten, Mechanisms of nutritional and hormonal regulation of lipogenesis, EMBO Rep. 2 (2001) 282–286.
[35] H. Zeng, H. Qin, M. Liao, E. Zheng, X. Luo, A. Xiao, Y. Li, L. Chen, L. Wei, L.J. Mm Zhao, CD36 promotes de novo lipogenesis in hepatocytes through INSIG2-dependent SREBP1 processing, Mol. Metab. 57 (2022) 101428.
[36] L.P. Bechmann, R.K. Gieseler, J.P. Sowa, A. Kahraman, J. Erhard, I. Wedemeyer, B. Emons, C. Jochum, T. Feldkamp, G.J.L.I. Gerken, Apoptosis is associated with CD36/fatty acid translocase upregulation in non-alcoholic steatohepatitis, Liver Intern. 30 (6) (2010) 850–859.
[37] H.A. Hostetler, A.B. Kier, F. Schroeder, Very-long-chain and branched-chain fatty acyl-CoAs are high affinity ligands for the peroxisome proliferator-activated receptor alpha (PPARalpha), Biochemistry 45 (24) (2006) 7669–7681.
[38] A. Yessoufou, W.J.Smw Wahli, Multifaceted roles of peroxisome proliferator-activated receptors (PPARs) at the cellular and whole organism levels, Swiss Med. Wkly. 140 (3738) (2010) w13071–w13071.
[39] T. Yoshikawa, T. Ide, H. Shimano, N. Yahagi, M. Amemiya-Kudo, T. Matsuzaka, S. Yatoh, T. Kitamine, H. Okazaki, Y.J.M.E. Tamura, Cross-talk between peroxisome proliferator-activated receptor (PPAR) α and liver X receptor (LXR) in nutritional regulation of fatty acid metabolism. I. PPARs suppress sterol regulatory element binding protein-1c promoter through inhibition of LXR signaling, Mol. Endocrinol. 17 (7) (2003) 1240–1254.
[40] F.A. Monsalve, R.D. Pyarasani, F. Delgado-Lopez, R.J.Moi Moore-Carrasco, Peroxisome proliferator-activated receptor targets for the treatment of metabolic diseases, Mediat. Inflamm. 2013 (1) (2013) 549627.
[41] J. Skat-Rørdam, D. Højland Ipsen, J. Lykkesfeldt, P. Tveden-Nyborg, A role of peroxisome proliferator-activated receptor γ in non-alcoholic fatty liver disease, Basic Clin. Pharm. Toxicol. 124 (5) (2019) 528–537.
[42] U.E. Lee, S.L.J.Bp Friedman, rC. gastroenterology, Mechanisms of hepatic fibrogenesis, Best. Pract. Res. Clin. Gastroenterol. 25 (2) (2011) 195–206.
[43] P. Horn, F.J.C.M. Tacke, Metabolic reprogramming in liver fibrosis, Cell Metab. (2024).
[44] J. Bates, A. Vijayakumar, S. Ghoshal, B. Marchand, S. Yi, D. Kornyeyev, A. Zagorska, D. Hollenback, K. Walker, K.J.Joh Liu, Acetyl-CoA carboxylase inhibition disrupts metabolic reprogramming during hepatic stellate cell activation, J. Hepatol. 73 (4) (2020) 896–905.
[45] T.T. Ross, C. Crowley, K.L. Kelly, A. Rinaldi, D.A. Beebe, M.P. Lech, R.V. Martinez, S. Carvajal-Gonzalez, M. Boucher, D.J.C. Hirenallur-Shanthappa, M. Gastroenterology, Hepatology, acetyl-CoA carboxylase inhibition improves multiple dimensions of NASH pathogenesis in model systems, Cell. Mol. Gastroenterol. Hepatol. 10 (4) (2020) 829–851.
[46] H. Jia, J. Liu, T. Fang, Z. Zhou, R. Li, W. Yin, Y. Qian, Q. Wang, W. Zhou, C.J. Sa Liu, The role of altered lipid composition and distribution in liver fibrosis revealed by multimodal nonlinear optical microscopy, Sci. Adv. 9 (2) (2023) eabq2937.
[47] Y. Zhang, S. Guo, C. Xie, J.J.Bri Fang, Uridine metabolism and its role in glucose, lipid, and amino acid homeostasis, BioMed. Res. Int. 2020 (1) (2020) 7091718.
[48] D. Cao, J.J. Leffert, J. McCabe, B. Kim, G. Pizzorno, Abnormalities in uridine homeostatic regulation and pyrimidine nucleotide metabolism as a consequence of the deletion of the uridine phosphorylase gene, J. Biol. Chem. 280 (22) (2005) 21169–21175.
[49] T.T. Le, A. Ziemba, Y. Urasaki, E. Hayes, S. Brotman, G.J.Jolr Pizzorno, Disruption of uridine homeostasis links liver pyrimidine metabolism to lipid accumulation, J. Lipid Res. 54 (4) (2013) 1044–1057.
[50] K.E. Sullivan, S. Kumar, X. Liu, Y. Zhang, E. de Koning, Y. Li, J. Yuan, F.J.S.R. Fan, Uncovering the roles of dihydropyrimidine dehydrogenase in fatty-acid induced steatosis using human cellular models, Sci. Rep. 12 (1) (2022) 14109.
[51] Y. Liu, C. Xie, Z. Zhai, Z.-Y. Deng, H.R. De Jonge, X. Wu, Z.J.F. Ruan, Function, Uridine attenuates obesity, ameliorates hepatic lipid accumulation and modifies the gut microbiota composition in mice fed with a high-fat diet, Food Funct. 12 (4) (2021) 1829–1840.
[52] E.F.G. da Silva, B.P. Costa, M.T. Nassr, B. de Souza Basso, M.S. Bastos, G. L. Antunes, C.K. Reghelin, M.C.R. Garcia, V.G.S. Levorse, L.P. Carlessi, Therapeutic effect of uridine phosphorylase 1 (UPP1) inhibitor on liver fibrosis in vitro and in vivo, Eur. J. Pharmacol. 890 (2021) 173670.
[53] W.V. Zheng, Y. Li, X. Cheng, Y. Xu, T. Zhou, D. Li, Y. Xiong, S. Wang, Z.J.Jo.C. Chen, M. Medicine, Uridine alleviates carbon tetrachloride-induced liver fibrosis by regulating the activity of liver-related cells, 26(3) (2022) 840–854.
[54] S.A. Yi, S. Sepic, B.A. Schulman, A. Ordureau, H. An, mTORC1-CTLH E3 ligase regulates the degradation of HMG-CoA synthase 1 through the Pro/N-degron pathway, Mol. Cell 84 (11) (2024) 2166–2184, e9.
[55] Y. Zhang, S. Guo, C. Xie, J. Fang, Uridine metabolism and its role in glucose, lipid, and amino acid homeostasis, BioMed. Res. Int. 2020 (1) (2020) 7091718.